

Network design for mesoscale inversions of CO₂ sources and sinks

By T. LAUVAUX^{1*}, A. E. SCHUH^{2,5}, M. BOCQUET³, L. WU^{3,4}, S. RICHARDSON¹, N. MILES¹ and K. J. DAVIS¹, ¹*Department of Meteorology, The Pennsylvania State University, University Park, TX, USA;* ²*Natural Resource Ecology Laboratory, Colorado State University, Fort Collins, CO, USA;* ³*CEREA, Joint Laboratory Ecole Nationale des Ponts et Chaussées/EDF R&D, Champs sur Marne, France;* ⁴*Laboratoire des Sciences du Climat et de l'Environnement, IPSL-LS, CECEA-CNRS-UVSQ, UMR8212, Saclay, France;* ⁵*Department of Atmospheric Science, Colorado State University, Fort Collins, CO, USA*

(Manuscript received 4 March 2012; in final form 26 April 2012)

ABSTRACT

Recent instrumental deployments of regional observation networks of atmospheric CO₂ mixing ratios have been used to constrain carbon sources and sinks using inversion methodologies. In this study, we performed sensitivity experiments using observation sites from the Mid Continent Intensive experiment to evaluate the required spatial density and locations of CO₂ concentration towers based on flux corrections and error reduction analysis. In addition, we investigated the impact of prior flux error structures with different correlation lengths and biome information. We show here that, while the regional carbon balance converged to similar annual estimates using only two concentration towers over the region, additional sites were necessary to retrieve the spatial flux distribution of our reference case (using the entire network of eight towers). Local flux corrections required the presence of observation sites in their vicinity, suggesting that each tower was only able to retrieve major corrections within a hundred of kilometres around, despite the introduction of spatial correlation lengths (~100 to 300 km) in the prior flux errors. We then quantified and evaluated the impact of the spatial correlations in the prior flux errors by estimating the improvement in the CO₂ model-data mismatch of the towers not included in the inversion. The overall gain across the domain increased with the correlation length, up to 300 km, including both biome-related and non-biome-related structures. However, the spatial variability at smaller scales was not improved. We conclude that the placement of observation towers around major sources and sinks is critical for regional-scale inversions in order to obtain reliable flux distributions in space. Sparser networks seem sufficient to assess the overall regional carbon budget with the support of flux error correlations, indicating that regional signals can be recovered using hourly mixing ratios. However, the smaller spatial structures in the posterior fluxes are highly constrained by assumed prior flux error correlation lengths, with no significant improvement at only a few hundreds of kilometres away from the observation sites.

Keywords: carbon dioxide, atmospheric inversion, air–land interaction, mesoscale modelling, carbon cycle, data assimilation

1. Introduction

The remaining fraction of atmospheric carbon from anthropogenic emissions corresponds to about 45% of the total emissions, due to absorption mechanisms on the continents and the oceans (Raupach et al., 2008; LeQuéré et al., 2009). Although anthropogenic emissions are re-

ported with high accuracy at the national level (Gurney et al., 2009), the role of continental surfaces affected by a large interannual variability remains critical to better understand and predict the atmospheric accumulation (Canadell et al., 2007). Their contribution remains poorly constrained at the continental and regional levels using inverse approaches despite consistency at larger scales (Ciais et al., 2010). Process-based approaches and statistical regression methods for parameter optimisation have also been used to constrain the carbon pools and the net flux from the terrestrial vegetation (Ricciuto et al., 2011),

*Corresponding author.
email: lauvaux@meteo.psu.edu

but large discrepancies remain on the annual and seasonal time scales (Keenan et al., 2012).

Because of the absence of direct measurements of regional carbon fluxes, the evaluation of the methods at policy relevant scales (few 10ths of kilometres) is limited to intermodel comparisons (Schwalm et al., 2010) and uncertainty analysis of parameters (Knorr and Heimann, 2001) or based on direct or indirect measurements (Wang et al., 2001). The Mid Continent Intensive (MCI) experiment focused on an intensively managed area for which agricultural inventories can provide reliable annual flux estimates (West et al., 2011), primarily driven by harvest production of crops. The inventory product can be used to evaluate other carbon flux estimates from biogeochemical terrestrial models, model-data fusion approaches, or atmospheric inversions. Despite the high precision obtained in the inventories from the collected crop harvest data (Ogle et al., 2010), the uncertainty over the entire region is increased by lower sampling frequency in the forest inventory, the parameterisations involved in the inventory models, the high variability from natural ecosystems and poorly documented semi-managed ecosystems such as pasture.

Mesoscale atmospheric inversions were used in several studies as a promising tool to monitor and estimate regional flux balances at high resolution (Lauvaux et al., 2009; Schuh et al., 2010; Göckede et al., 2010a). Though errors in the atmospheric transport model and at the boundaries limit the potential of the method (Göckede et al., 2010b; Lauvaux et al., 2012), mesoscale inverse systems have shown consistent improvements from prior fluxes over short periods of time (Lauvaux et al., 2009), and at the annual time scale over the region (Schuh et al., 2010). Over longer time scales, the assessment of the regional flux balance implies the capability of capturing the spatio-temporal variability in the atmospheric CO₂ mixing ratios and avoiding persistent errors from the atmospheric transport models (e.g. Gerbig et al. 2006). Although prior fluxes, uncertainty assessment and transport models are evaluative components of the system, the deployment strategy of observation sites affects the potential of the inversion indefinitely.

The design of regional atmospheric networks amounts to the optimisation of the observational constraint on the surface fluxes from the atmospheric concentrations. The atmospheric integrator effect is one part of the answer, and actual footprints of hourly tower concentration data were shown to constrain mainly the few hundreds of kilometres around each site (Lauvaux et al., 2008; Gerbig et al., 2009). Even though large-scale signals are present in the concentrations, their relative contribution being 20–40% (depending on the season) of the observed hourly variability (Miles et al., 2012), but the corresponding flux area is so large that

very little information is carried by the data to constrain the flux per surface unit. In addition, CO₂ fluxes show large diurnal patterns varying from negative values during the day to positive during the night (photosynthesis and respiration), resulting in a substantial loss of information at the daily time scale (Gerbig et al., 2009). Still, regional-scale signals and redundant flux signatures in the atmospheric concentrations might inform us about larger flux balances, depending on the site location and the strength of the local fluxes.

Previous studies have demonstrated the relative contribution of the near-field fluxes in the hourly atmospheric observations using a limited number of observation sites deployed over short periods of time (Lauvaux et al., 2009). Other studies have used similar modelling tools at coarser resolution but for non-CO₂ trace gases, *i.e.* those not affected by diurnal cycles, and limited by the resolution to extract the high time frequency atmospheric information from the observations (Gloor et al., 2001). In addition to the use of high-frequency data, the a priori flux spatial distribution in the region of interest is the second major element. Once combined in the inverse system, both determine the potential of convergence to assess the regional carbon balance and the capability to retrieve the correct spatial flux distribution. The convergence of the system is directly related to the spatial and temporal resolutions of the aggregated fluxes. The aim is to constrain the surface fluxes which is different from observing signals from different scales in the observations. The relative contribution of one scale can limit the use of the others. A crucial element of the inverse system concerns the detection of major discrepancies in the prior fluxes. These are not detectable by any pseudo-data sensitivity study without prior knowledge of potential biases or errors in the prior fluxes. If towers are to be deployed, the design of the network is based on its ability to capture surface flux discrepancies at any place in the domain. Networks that are too sparse might have limited potential, whereas too dense networks are cost-prohibitive and harder to maintain on a long-term basis. Basically, the distance between observation sites and critical flux areas has to be determined within an inverse framework, such that atmospheric signals are strong enough to optimise the regional fluxes relatively to other contributors.

We propose here a set of tests based on previous results over the MCI area (Lauvaux et al., 2012) using different combinations of tower sites, considering their impacts on the regional flux balance and its spatial distribution. We focus on June to December 2007 which allows us to (1) evaluate the weight of the observations from each site to help constrain the regional carbon balance and its spatial distribution and (2) investigate the impact of different prior error statistics that may be used in network design studies

and evaluate our own assumptions. This step is critical before using the error reduction as a reliable estimate for network design purposes; furthermore, a large correlation length in the prior flux errors can lead to over-constrained systems (or under-estimated posterior uncertainties).

2. Methods

2.1. The campaign and the modelling tools

For this study, we used eight CO₂ mixing ratio tower sites that were deployed for the MCI experiment (Miles et al., 2012). Two towers are part of the permanent tall tower NOAA network, LEF and WBI; five sites were instrumented for the campaign, Kewanee, Round Lake, Mead, Galesville, Centerville; and the last site is the calibrated flux tower Missouri Ozarks [cf. Fig. 1(a)]. The inverse system, described in a previous study (Lauvaux et al., 2012), uses WRF-Chem meteorological fields at 10 km resolution to drive the Lagrangian Particle Dispersion Model (Uliasz, 1994) and generates the concentration footprints over the entire period of observations. The prior fluxes were simulated with the SiBcrop model, with an improved phenology for crops based on several eddy-flux sites over the MCI (Lokupitiya et al., 2009). The inverse CO₂ fluxes are at 20 km resolution over the domain at a weekly time step. We solve for two flux components (one for daytime and one for nighttime). We also solve for boundary condition concentrations from the CarbonTracker system corrected by aircraft data (Lauvaux et al., 2012). The boundary conditions are additional unknowns here but in practice act as an additional source of uncertainties, reducing the overall error reduction of the different cases equally.

2.2. Inverse methodology

The method used in the paper was described in the study of Lauvaux et al. (2012). The state vector (\mathbf{x}) that includes the three components described above (daytime fluxes, nighttime fluxes and boundary inflow) is obtained by the following equation:

$$\mathbf{x} = \mathbf{x}_0 + \mathbf{B}\mathbf{H}^T(\mathbf{H}\mathbf{B}\mathbf{H}^T + \mathbf{R})^{-1}(\mathbf{y} - \mathbf{H}\mathbf{x}_0) \quad (1)$$

where \mathbf{x} are the unknown fluxes and the boundary conditions we invert for, \mathbf{x}_0 the a priori flux and boundary estimates, \mathbf{y} the observations, \mathbf{H} the linearised transport matrix and \mathbf{R} and \mathbf{B} the error covariance matrices of the observations and the a priori fluxes, respectively.

We can define the posterior error covariance matrix \mathbf{A} for fluxes given by the following expression:

$$\mathbf{A}^{-1} = \mathbf{B}^{-1} + \mathbf{H}^T\mathbf{R}^{-1}\mathbf{H} \quad (2)$$

In the study, we perform error reduction analyses as if exploring optimal tower locations for a network design study. The error reduction is the ratio between flux error variances before and after inversion $[1 - (\sigma_A/\sigma_B)]$ with values ranging from 0 to 1, with σ_A the posterior flux root mean square error (RMSE) and σ_B the prior flux RMSE. A value of 0 indicates no improvement of the initial prior errors. Between 0 and 1, the value is interpreted as a ratio of error reduction, referred in percentage in this study.

In addition, we define prior flux error structures in two different ways: first by considering the ecosystem distribution in space and a correlation length L , and second only by the correlation length L (Lauvaux et al., 2012). The distance L remains difficult to rigorously estimate but its impact on the retrieved fluxes can be large (Wu et al., 2011). Additional tests will be performed based on our subsampled network inversions, to evaluate the impact of the flux corrections on the CO₂ concentration mismatch of the observation sites not used in the inversion.

2.3. Evaluation of the assumptions in spatial structures of the prior flux errors

2.3.1. Ratio between the observational constraint and prior flux errors. To evaluate the impact of the correlation structures on the solutions, we use the degree of freedom for the signal (DFS) from Rodgers (2000). A large (respectively, small) correlation length reduces (respectively, increases) the DFS. The DFS was defined following Bocquet (2009) as:

$$\text{DFS} = \text{Tr}(\mathbf{B}\mathbf{H}^T(\mathbf{H}\mathbf{B}\mathbf{H}^T + \mathbf{R})^{-1}\mathbf{H}) \quad (3)$$

The DFS is used in this study to investigate the impact of the correlation length on the solutions. Small DFS values compared to the number of observations indicates that the posterior fluxes are constrained mainly by the prior uncertainties. Large correlation lengths lead to less information brought by the observations. We discuss the DFS values in Section 4.

The variances in the prior flux errors vary slightly from one case to the next to conserve the same ratio between the observational constraint and the prior flux uncertainties. This balance was ensured by estimating the normalised distance λ of the χ^2 test as follows:

$$\lambda = \frac{1}{n}[(\mathbf{y} - \mathbf{H}\mathbf{x}_0)^T(\mathbf{H}\mathbf{B}\mathbf{H}^T + \mathbf{R})^{-1}(\mathbf{y} - \mathbf{H}\mathbf{x}_0)] \quad (4)$$

with n the degree of freedom of the state vector. A value close to one indicates reasonable estimates of prior errors in the inverse system, balancing the weight of the atmospheric observations and their related errors (\mathbf{y} and \mathbf{R}) compared with the initial uncertainties in the fluxes (\mathbf{x}_0 and \mathbf{B}) and

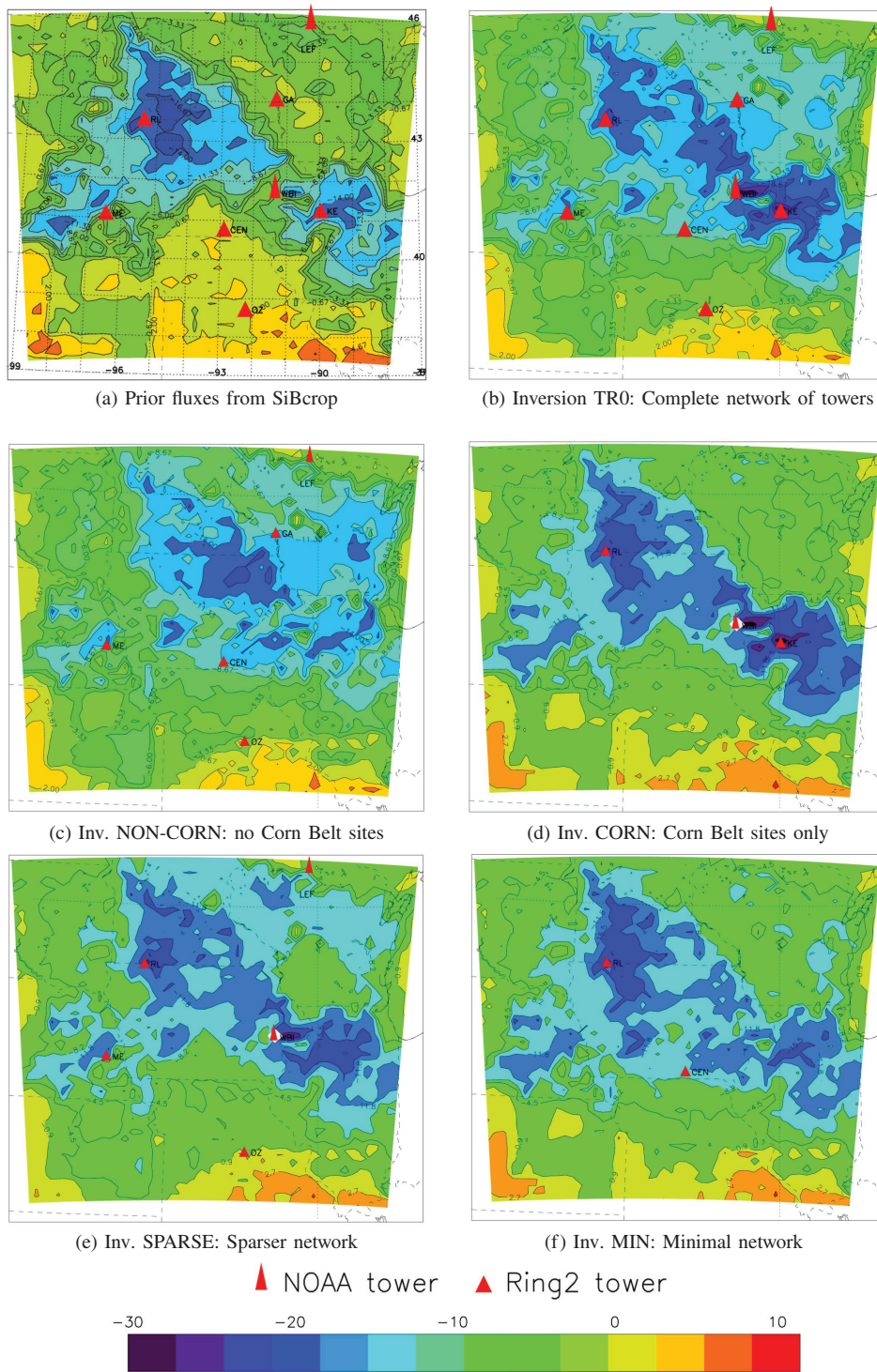


Fig. 1. CO_2 fluxes from June to December in $\text{TgC}\cdot\text{degree}^{-2}$ over the MCI from the SiBcrop vegetation model (a), our reference case TR0, i.e. the inverse system using the entire network of observation sites (b), using only the sites outside of the Corn Belt area (c), using the sites only within the Corn Belt area (d), using a sparser network (e) and using a minimal configuration of two sites (one in the Corn Belt and one out) (f).

the number of independent elements in the state vector. The values of λ range between 0.75 and 1.25 for all our tests, and the corresponding correlation lengths from 50 to 300 km, including both biome-dependent and non-biome-dependent structures. We increase (or decrease) the RMS (diagonal elements of \mathbf{B}) to compensate for changes in the correlation length based on the values of lambda for each case.

2.3.2. Leave-One-Out Cross-Validation. We evaluated the gain from the inversion in terms of mixing ratio mismatch with Leave-One-Out Cross-Validation (LOOCV) tests. We performed eight consecutive inversions using seven of the eight available tower sites. The remaining site is used as a validation of the inverse fluxes. The simulated mixing ratios of the validation site are reconstructed using its influence functions and the fluxes from the corresponding 7-tower inversion. The mixing ratio mismatch at the validation site i ($\Delta_i = \mathbf{y} - \mathbf{H}\mathbf{x}_i$) is computed before ($\mathbf{x}_i = \mathbf{x}_0$) and after inversion ($\mathbf{x}_i = \mathbf{x}$). The mean of the mismatch represents the impact of the correction of weekly biases in the observation space (mixing ratios). The RMSE of hourly mismatches represents smaller-scale corrections (from hourly mixing ratios) produced by changing wind conditions at each site. These tests provide an assessment of the overall gain after inversion, gain from corrections on the weekly fluxes and in space around the validation site. Considering that most tower mixing ratio footprints do not overlap between sites, the LOOCV evaluates primarily the veracity of the spatial correlation in the prior flux errors.

3. Results

The amount of information from the observation network varies with two major elements: the spatial density of the network and the correlations of the prior flux errors.

To explore these two components, first we define several subnetworks using only some of the eight available sites, and second, we assume different prior flux error structures with an evaluation of their impact.

3.1. Regional CO₂ flux balance

In this section, we diagnose the information content of the observations using different combinations of sites to constrain the regional balance. We defined four cases as follows: the first network excludes sites in the corn belt (Round Lake, West Branch and Kewanee) referred here as NON-CORN; the second case uses sites within the corn belt only (the ones previously excluded) referred as CORN; a sparser network of observations but homogeneously distributed in space (excluding Centerville, Galesville and Kewanee) referred as SPARSE; and finally the minimum configuration with one site in the corn belt area and one for the mixed grassland-crop-forest area, Round Lake and Centerville, referred as MIN.

We present the inversion-based regional balances using the different network configurations as shown in Table 1. Table 1 underlies the capacity of the system to constrain the overall regional balance of the MCI domain and displays the averaged CO₂ fluxes over corn-dominated areas and non-corn-dominated areas to highlight the attribution of flux corrections over the domain in the two most distinct vegetated areas. Considering the MIN case, the density of the network is apparently not the main leverage to constrain the regional balance. Only two towers are used in this case, and the final balance and area averaged fluxes are close to the initial full network inversion result (about 30 TgC difference or less than 1-sigma from the posterior uncertainties). In the CORN case using three sites in the corn belt area, we observe that the correction is weaker (only -49 TgC instead of -84 TgC). The locations of the

Table 1. Regional CO₂ flux balance from June to December 2007 in TgC over the MCI (first line), and averaged fluxes over the corn-dominated area (which corresponds to 23% of the domain) and out of it in gCm⁻², for Sibcrop (prior fluxes), using the complete observation network (posterior or TR0), using towers around the corn belt (NON-CORN), using towers within the corn belt area (CORN), using a sparser network of towers (SPARSE), and using only two towers (MIN)

	Prior	Posterior (TR0)	NON-CORN (five sites)	CORN (three sites)	SPARSE (five sites)	MIN (two sites)
Regional carbon balance (TgC)	-110	-194	-179	-159	-185	-177
Total flux error (TgC)	35.5	32.1	32.7	33.1	32.5	33.6
Corn area averaged flux (gCm ⁻²)	-335.7 ± 98.6	-343.84 ± 88.16	-280.62 ± 92.39	-372.38 ± 88.92	-328.9 ± 89.56	-336.85 ± 92.03
Out-of-corn averaged flux (gCm ⁻²)	-27.3 ± 36.13	-110.71 ± 32.86	-114.49 ± 32.87	-69.56 ± 34.75	-108.23 ± 33.26	-97.75 ± 34.55

towers seem more important than the absolute number of sites. Considering the averaged fluxes over corn-dominated areas and grass-dominated areas, the complete network case (referred here as posterior) indicates a slight increase of the uptake in corn-dominated areas and an important increase elsewhere (cf. Table 1). The posterior uncertainties over the domain for the different cases vary from 5 to 10% error reduction compared to the initial uncertainties. A large fraction of the domain being unconstrained by the observations, the error reduction is relatively small for the different cases. Although most cases as can be seen in Table 1 show similar flux corrections for the corn area (between the prior and posterior values), the NON-CORN case shows here an opposite flux correction in the corn area due to the absence of observation sites. We investigate the spatial distribution of the corrections in the next section.

3.2. Spatial flux distributions

The spatial distribution of the corrections appears critical around the central Corn Belt, and the net fluxes averaged over the corn area remains similar (Table 1). The initial spatial distribution (prior flux) was centred and highly correlated with the corn-dominated area [Fig. 1(a)]. In the posterior fluxes, the sink area is extended to the South (northern Missouri) and to the North–West and North–East (South Dakota and Wisconsin) [cf. Fig. 1(b)].

With the inversion including only corn sites [Fig. 1(d)], the averaged fluxes in the non-corn-dominated areas show the smallest increase in uptake. The uptake in the north-eastern part of the domain remains low [case CORN and MIN, or (d) and (f) in Fig. 1]. In the other cases, both Galesville and LEF towers introduce an increase of the uptake [NON-CORN and SPARSE, or (c) and (e) in Fig. 1], *i.e.* extending the sink area to the North East. The most variable and important change compared to the initial setup occurs in northern Illinois where there is the largest uptake in the posterior fluxes [Fig. 1(b)]. Comparatively, the prior fluxes showed a maximum around Round Lake in northern Iowa and southern Minnesota [Fig. 1(a)]. The maximum in Illinois is present only if the Kewanee or West Branch sites are included [CORN and SPARSE, or (d) and (e) in Fig. 1]. Other cases produce the maximum of uptake in northern Iowa and southern Minnesota (MIN), or decrease the uptake but without detecting the northern Illinois area (NON-CORN). The tower sites at Centerville or Galesville are located about 300 km from northern Illinois but do not produce an increase in uptake.

3.3. Spatial distribution of flux corrections

We present the flux corrections shown in Fig. 2 to highlight the contribution of different combination of towers applied to the prior fluxes. Across the four cases, the main spatial patterns are conserved indicating consistent corrections across towers. The only case which indicates a disagreement between tower corrections is NON-CORN, with an important positive correction around Round Lake. The presence of Round Lake in the other cases induces little to no change around the tower location. Overall, the intensity of these changes is highly variable. In most cases, the large uptake around Round Lake is decreased, the NON-CORN case being the most positive correction in this area. Once again, the corrections appear only when towers are in the area of interests (*e.g.* the negative correction around Centerville in NON-CORN and MIN) or when two towers surround the area (Ozarks and WBI also decrease the Centerville area in SPARSE). The positive correction around Round Lake is produced in all cases. Otherwise, the corrections disappear if the closest tower is missing. As an illustration of the prior error correlation impact on the retrieved fluxes, the Fig. 2(b) shows the flux corrections if biome-related structures are removed from the prior errors. We will discuss this point in Section 4.

3.4. Theoretical error reduction and observed flux corrections

We now consider an experimental network design based on the error reduction only. We compare here the theoretical benefits from our system (without using observations) to the actual changes in the posterior fluxes (with observations). Because the two are basically related to the prior flux error structures, we investigate the impact of different correlation structures on the flux corrections and the error reduction. The impact of the prior fluxes themselves was investigated in the study of Lauvaux et al. (2012).

The reference setup TR0 includes all the towers in the region and flux error covariances based on ecosystems and distance ($L = 300$ km). The error covariances are based on model-data mismatch and correlation analysis using several eddy-flux sites over the domain (Lauvaux et al., 2012). As a comparison, for a similar correlation length but without considering ecosystems, the overall constraint in our system is equivalent to $L = 100$ km. The biome dependence, as defined here, reduces the initial correlation length (cf. Fig. 3). We then ran our 7-month inversion at the weekly time scale. The error reduction in Fig. 3(a) is about 30–40% in the vicinity of the towers and about 10–20% in the first 100–200 km. We then ran a second inversion (case TRD)

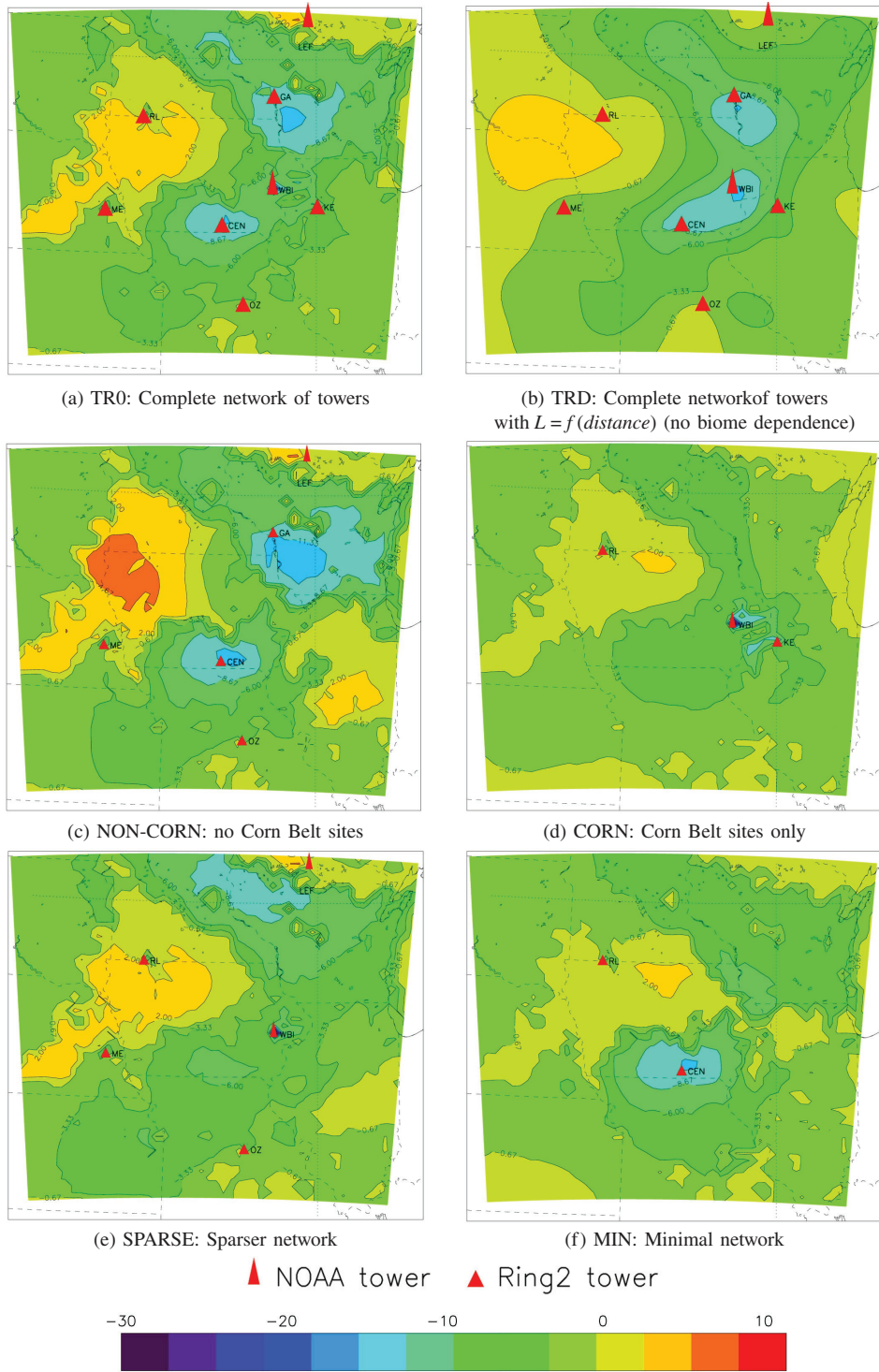


Fig. 2. CO₂ flux correction from June to December in TgC.degree⁻² over the MCI using the SiBcrop prior fluxes, with our reference case, i.e. the inverse system using the entire network of observation sites (a), with the entire network but the flux error correlation is built on an exponentially decreasing model only (b), using only the sites out of the Corn Belt area (c), using the sites only within the Corn Belt area (d), using a sparser network (e) and using a minimal configuration of two sites (one in the Corn Belt and one out) (f).

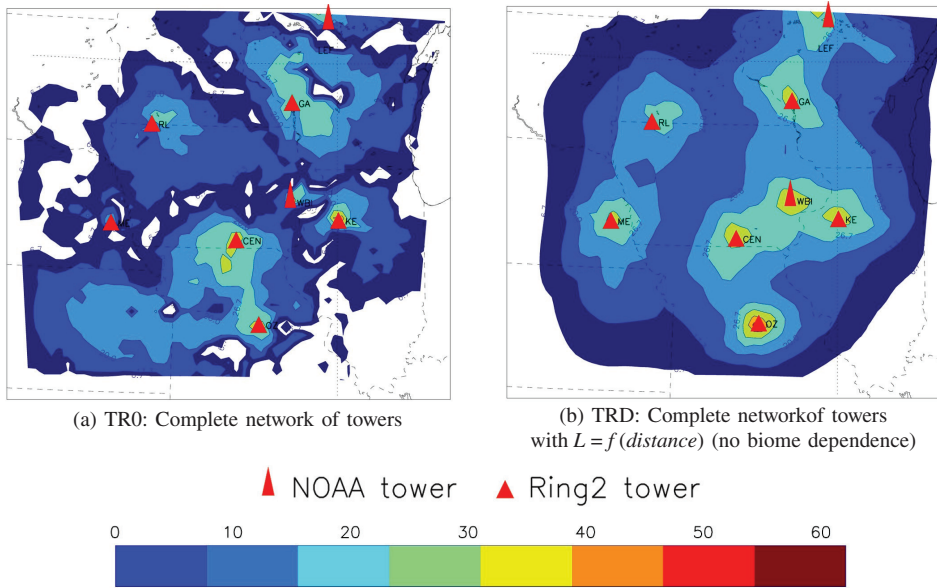


Fig. 3. Error reduction in % using all the towers and prior flux errors with ecosystem-based standard deviations (RMS) and spatial correlations based on ecosystems and distances between pixels (case TR0) (a) and the second case considering correlations with distance only (exponentially decaying model) (TRD) (b).

using the same standard deviations for every 20 km by 20 km pixels, but prior flux error correlations are based on the distance only, with an exponentially decaying model ($L = 300$ km). The simpler structure of the prior flux errors here induces the propagation of corrections in space from grass to corn dominated pixels for example. This assumption seems somewhat unrealistic as Net Ecosystem Exchange (NEE) for corn is driven by a different phenology and several human-driven processes such as irrigation or fertilisation. Corrections applied to corn-dominated pixels might not be applicable to grassland areas as vegetation responses and error sources might be highly variable across these ecosystems. The spatial distribution of the error reduction [Fig. 3(a) and (b)] for the two cases shows large differences. The second case (TRD) shows exponentially decreasing error reduction from the tower locations as prescribed by the error correlations.

The flux corrections from these two cases [cf. Fig. 2(a) and (b)] show clear differences even though their respective regional carbon balances remain close, with -194 TgC for the TR0 case and -179 TgC for the TRD case. Posterior uncertainties and fluxes are highly affected by the assumptions in the prior error statistics even if the main patterns remain somehow similar. The posterior flux errors for the TR0 case are about 32 TgC (with 35.5 TgC error in the prior fluxes), whereas the TRD case posterior errors are about 25.2 TgC (with an error of 30.5 TgC in the prior fluxes). The relationship between prior error structures and posterior errors and fluxes has a consequent impact on the

flux errors, but little impact on the regional carbon balance (posterior fluxes). In Section 4, we investigate the observational constraint and the validity of the flux error correlation assumption by estimating the degree of freedom of the signals (DFS) (Rodgers, 2000; Bocquet, 2009) and by evaluating the flux corrections on towers that were not used in the inversion from our different cases (LOOCV).

4. Discussion

4.1. Optimal choice of prior error structures

The different inversions performed here and their interpretation are highly dependent on the prior error covariances. Wu et al. (2011) noted the impact of incorrect flux error correlations in the prior error covariance matrix. The definition of prior error structures in space remains difficult to estimate quantitatively, and several studies discussed the estimation of the potential correlations using different techniques. Although geostatistical approaches propose to diagnose these structures from different observational datasets (Michalak et al., 2005), other inverse studies have optimised these distances based on correlation analysis of biogeochemical models (Rödenbeck et al., 2003; Chevallier et al., 2006) or derived them from climatological and ecological considerations (Peters et al., 2007). At large scale, the ill-conditioning of the inverse problem leads to significantly long spatial flux error correlations in order to keep a sufficient observational constraint. Here, a large

number of observations and the relatively short distances between sites tend to rapidly reduce the DFS and lead to the convergence of the solutions. The estimation of flux error correlations, if they exist, is required to obtain precise estimates of the a posteriori flux errors. We performed several tests using only a subsample of the complete network, with several observation sites available for a cross-validation of the corrections. We considered here the case CORN, using only Round Lake, West Branch and Kewanee sites, the other five being used as independent observations to evaluate the flux corrections. We define three cases with different correlation structures, the first one using a correlation length of 300 km, exponentially decaying with the distance, and combined with the biome map of the region (Lauvaux et al., 2012) (referred here as TR0), then a second case using correlation length of 300 km only (TRD) and finally a third case with a correlation length of 50 km (L₅₀). We estimated the gain in terms of the final CO₂ concentration mismatch compared to the initial (a priori) model-data mismatch at the five remaining towers, in ppm. Over the 28 periods of inversions from June to December, the gain for the cases TR0 or TRD improves the initial mismatch by 0.823 and 0.861 ppm, respectively, compared to the case L₅₀ with only 0.561 ppm. On average, the simpler exponentially decaying model (=TRD) shows a larger gain compared to the more complex vegetation-based description TR0, but 4 of the 28 periods show small net degradations of the initial mismatch, against two for the TR0 case. Similarly, the DFS drops from 284 for the case L₅₀, and 281 for the TR0 case, down to 59 for the case TRD, indicating an important increase of the apparent observational constraint due to the correlation length in the flux errors. This first analysis shows that the larger flux correlations of 300 km seems the

most profitable assumption in terms of gain. But the presence of degradation of several periods (4 out of 28) indicates that more refinement is required, including temporal variability for example. The gain increasing with the correlation length might also correspond to the overall decrease of the regional flux bias. This overall gain remains valid at the regional scale, but the inherited structures in space in the posterior fluxes might be artificial, constrained by the assumed correlation length more than the data and their adjoint transport.

4.2. Cross-validation of posterior fluxes

We performed LOOCVs to evaluate the gain at each tower in terms of the CO₂ concentration mismatch. The principle of cross-validation relies on eight inversions using seven towers only out of the eight available concentration sites. The retrieved fluxes are then propagated through the influence function of the validation tower. The improvement in the concentration mismatch at the eliminated tower is a direct evaluation of the posterior fluxes. We computed both RMSEs and means for each of the inversions with a different validation tower. This analysis evaluates the assumptions made in the prior flux errors (spatial correlation) in terms of systematic error corrections and sub-weekly corrections (RMSE). The results are presented in Table 2. The means show that all the inversions, but one provides smaller mismatch at the validation tower. We conclude here that the inversion improved the fluxes in terms of systematic errors at the weekly timescale. In terms of RMSE, the results indicate no or little decrease in the concentration mismatch compared to the reference inversion (using the eight concentration towers), with an increase of the mismatch in three cases. The absence of

Table 2. Mixing ratio residuals in ppm for each tower, averaged over the 7 months (mean) and their related RMSE at the hourly time scale before and after inversion. The three lines correspond to the initial mismatch between modelled and observed mixing ratios (a priori), posterior residuals after inversion using the eight towers (a posteriori) and residuals from each inversion excluding the tower indicated in the first line, used for validation (LOOCV)

	Centerville	Kewanee	Round Lake	Mead	Galesville	Missouri	WBI	LEF
A priori								
Mean	-1.708	-1.248	-0.583	-1.025	-1.912	-0.578	-1.203	-0.167
RMSE	7.641	7.169	7.284	6.858	7.970	7.884	8.341	6.786
A posteriori								
Mean	-0.103	-0.028	-0.104	-0.074	-0.162	0.102	0.467	0.171
RMSE	3.711	3.757	3.638	3.511	4.244	4.067	4.269	3.837
LOOCV								
Mean	-1.045	-0.283	-0.613	-0.883	-1.371	-0.119	0.235	0.865
RMSE	7.003	7.564	7.479	6.794	7.602	7.727	7.656	7.848

Residuals in LOOCV correspond to cross-validation of the inverse fluxes retrieved from the Leave-One-Out experiments. Values closer to zero compared with the a priori mismatch indicate an improvement.

improvement in the RMSE shows that the subweekly variability due to smaller-scale flux signals is not captured correctly compared to the reference inversion. The spatial error correlation might be over-estimated in our setup, even though the regional balance with fewer towers is consistent with previous findings. The small structures in the flux corrections are not realistic at the validation tower. The extent of corrections in space is artificial and only helps to improve larger-scale systematic errors. However, the two inversions without WBI or Keweenaw show almost identical improvements compared to the reference inversion in terms of means of the mismatch. The redundancy of the information from these two towers is in agreement with earlier findings, co-located in the corn belt area.

4.3. Estimation of prior error structures

From our analysis, we can disaggregate two correction terms from the flux correction, one due to local atmospheric signals, and one induced by the presence of spatial correlations in the prior flux errors. The second seems consistent following our previous tests. Even if not perfect, long correlation lengths ($L \sim 300$ km) showed an improvement compared to the initial CO₂ concentration mismatch, and better results than smaller correlation lengths ($L \sim 50$ km). For the first term, the simulated atmospheric mixing drives primarily the size of the main area of influence on the concentrations. The model resolution might affect the dimensions of the concentration footprints noting that horizontal diffusion is related to model parameterisation optimised at given resolutions. Comparisons are needed to explore the sensitivity of the footprint size to the model configuration. Although the two terms might seem contradictory, they reflect two different facts. The first term represents directly observed flux signals in the atmospheric concentrations. The second term represents the common sources of errors in the fluxes. This term is problematic in the sense that corrections are distributed spatially, even though the observations alone were not able to constrain these areas initially. Chevallier et al. (2006) investigated the presence of flux error correlations using eddy-flux sites, at a daily time scale. The temporal scale of this study was shorter than the present pixel-based inversion at the weekly time scale. They found no clear spatial structures in the prior flux errors. Hilton (2011) optimised parameters of a vegetation model with 100 eddy-covariance NEE measurement sites across North America and diagnosed the covariances in the residuals. The most likely correlation length was about 400 km at the monthly time scale and 200 km at the 10-day time scale. Before that, Rödenbeck et al. (2003) performed model sensitivity tests at the monthly time scale and diagnosed correlation lengths of

about 1200 km. Michalak et al. (2005) proposed the use of the Maximum Likelihood algorithm to derive prior flux error correlations based upon observations which were a direct result of those fluxes. While the method is very informative for the modellers to evaluate the balance of the inverse system, the reality of flux error correlations has to be investigated, not only to fit the inverse setup because of other limiting factors (model resolution, number of observations, dimension of the matrices to invert), but also to represent the real structures of the prior flux errors.

5. Conclusions

We have evaluated here the CO₂ posterior fluxes over the corn belt of the US Midwest by subsampling the MCI tower network. Atmospheric inversions at 20-km resolution were performed for a 7-month period, with similar assumptions but variable observational constraints. These sensitivity tests correspond to different network configuration, including a sparser network of observations or ecosystem-specific networks. The four different subsampled networks showed consistent regional carbon balances despite tower removals ($-178 \text{ TgC} \pm 13$). The DFS showed that the posterior fluxes are constrained mainly by flux error correlation when the correlation length is larger than 150 km. The gain in the final concentration mismatch indicates an improvement of the overall regional fluxes with large correlation length (300 km or more) but might correspond to artificial extension of the regional bias correction rather than realistic spatial structures in the posterior fluxes. This preliminary study shows that the MCI campaign provides a sufficient number of observations to constrain the Corn Belt carbon balance over the 7-month period, but the spatial distribution of the inverse fluxes is still under-constrained with too little observational constraint compared to the assumed flux error structures.

6. Acknowledgements

We thank Arlyn Andrews from NOAA/ESRL for providing the data from the West Branch tall tower site (WBI) and the WLEF tower (LEF). We thank Peter J. Rayner for fruitful discussions. This work was supported by the Office of Science (BER) US Department of Energy, Terrestrial Carbon Program, the US National Aeronautics and Space Administration's Terrestrial Ecology Program, the US National Oceanographic and Atmospheric Administration, Office of Global Programs and Global Carbon Cycle Program.

References

- Bocquet, M. 2009. Towards optimal choices of control space representation for geophysical data assimilation. *Mon. Weather Rev.* **137**, 2331–2348. Online at: <http://journals.ametsoc.org/doi/abs/10.1175/2009MWR2789.1>
- Canadell, J. G., Le Quéré, C., Raupach, M. R., Field, C. B., Buitenhuis, E. T. and co-authors. 2007. Contributions to accelerating atmospheric CO₂ growth from economic activity, carbon intensity, and efficiency of natural sinks. *Proc. Natl Acad. Sci.* **104**(47), 18866–18870. DOI: 10.1073/pnas.0702737104. Online at: <http://www.pnas.org/content/104/47/18866.abstract>
- Chevallier, F., Viovy, N., Reichstein, M. and Ciais, P. 2006. On the assignment of prior errors in Bayesian inversions of CO₂ surface fluxes. *Geophys. Res. Lett.* **33**, L13802. DOI: 10.1029/2006GL026496. Online at: <http://www.agu.org/pubs/crossref/2006/2006GL026496.shtml>
- Ciais, P., Rayner, P., Chevallier, F., Bousquet, P., Logan, M. and co-authors. 2010. Atmospheric inversions for estimating CO₂ fluxes: methods and perspectives. *Clim. Change* **103**(1/2), 69–92. DOI: 10.1007/s10584-010-9909-3. Online at: <http://www.springerlink.com/content/pnk685jh102375r0/>
- Gerbig, C., Dolman, A. J. and Heimann, M. 2009. On observational and modelling strategies targeted at regional carbon exchange over continents. *Biogeosciences* **6**(10), 1949–1956. DOI: 10.5194/bg-6-1949-2009. Online at: <http://www.biogeosciences.net/6/1949/2009/>
- Gerbig, C., Lin, J. C., Munger, J. W. and Wofsy, S. C. 2006. What can tracer observations in the continental boundary layer tell us about surface-atmosphere fluxes? *Atmos. Chem. Phys.* **6**(2), 539–554. DOI: 10.5194/acp-6-539-2006. Online at: <http://www.atmos-chem-phys.net/6/539/2006/acp-6-539-2006.html>
- Gloor, M., Bakwin, P., Hurst, D., Lock, L., Draxler, R. and co-authors. 2001. What is the concentration footprint of a tall tower? *J. Geophys. Res.* **106**, 17831–17840.
- Göckede, M., Michalak, A. M., Vickers, D., Turner, D. P. and Law, B. E. 2010a. Atmospheric inverse modeling to constrain regional scale CO₂ budgets at high spatial and temporal resolution. *J. Geophys. Res.* **115**, D15113. DOI: 10.1029/2009JD012257. Online at: <http://www.agu.org/pubs/crossref/2010/2009JD012257.shtml>
- Göckede, M., Turner, D. P., Michalak, A. M., Vickers, D. and Law, B. E. 2010b. Sensitivity of a subregional scale atmospheric inverse CO₂ modeling framework to boundary conditions. *J. Geophys. Res.* **115**, D24112. DOI: 10.1029/2010JD014443. Online at: <http://www.agu.org/pubs/crossref/2010/2010JD014443.shtml>
- Gurney, K. R., Mendoza, D., Zhou, Y., Fischer, M., Miller, C. and co-authors. 2009. High resolution fossil fuel combustion CO₂ emission fluxes for the United States. *Environ. Sci. Technol.* **43**(14), 5535–5541. Online at: <http://pubs.acs.org/doi/abs/10.1021/es900806c>
- Hilton, T. W. 2011. *Spatial Structure in North American Terrestrial Biological Carbon Fluxes and Model Errors Evaluated with a Simple Land Surface Model*. PhD Dissertation. The Pennsylvania State University. Online at: <http://etda.libraries.psu.edu/>
- Keenan, T. F., Baker, I., Barr, A., Ciais, P., Davis, K. and co-authors. 2012. Terrestrial biosphere model performance for inter-annual variability of land-atmosphere CO₂ exchange. *Glob. Change Biol.* **18**(6), 1971–1987. DOI: 10.1111/j.1365-2486.2012.02678.x.
- Knorr, W. and Heimann, M. 2001. Uncertainties in global terrestrial biosphere modeling, part II: global constraints for a process-based vegetation model. *Glob. Biogeochem. Cycl.* **15**, 227–246. Online at: <http://www.agu.org/pubs/crossref/2001/1998GB001060.shtml>
- Lauvaux, T., Gioli, B., Sarrat, C., Rayner, P. J., Ciais, P. and co-authors. 2009. Bridging the gap between atmospheric concentrations and local ecosystem measurements. *Geophys. Res. Lett.* **36**, L19809. DOI: 10.1029/2009GL039574. Online at: <http://www.agu.org/pubs/crossref/2009/2009GL039574.shtml>
- Lauvaux, T., Schuh, A. E., Uliasz, M., Richardson, S., Miles, N. and co-authors. 2012. Constraining the CO₂ budget balance of the corn belt: exploring uncertainties from the assumptions in a mesoscale inverse system. *Atmos. Chem. Phys.* **12**, 337–354. DOI: 10.5194/acp-12-337-2012. Online at: <http://www.atmos-chem-phys.net/12/337/2012/acp-12-337-2012.html>
- Lauvaux, T., Uliasz, M., Sarrat, C., Chevallier, F., Bousquet, P. and co-authors. 2008. Mesoscale inversion: first results from the Ceres campaign with synthetic data. *Atmos. Chem. Phys.* **8**(13), 3459–3471. DOI: 10.5194/acp-8-3459-2008. Online at: <http://www.atmos-chem-phys.net/8/3459/2008/>
- LeQuéré, C., Raupach, M. R., Canadell, J., Marland, G., Bopp, L. and co-authors. 2009. Trends in the sources and sinks of carbon dioxide. *Nat. Geosci.* **2**, 831–836. DOI: 10.1038/ngeo689. Online at: <http://www.nature.com/ngeo/journal/v2/n12/abs/ngeo689.html>
- Lokupitiya, E., Denning, S., Paustian, K., Baker, I., Schaefer, K. and co-authors. 2009. Incorporation of crop phenology in Simple Biosphere Model (SiBcrop) to improve land-atmosphere carbon exchanges from croplands. *Biogeosciences* **6**, 969–986. DOI: 10.5194/bg-6-969-2009. Online at: <http://www.biogeosciences.net/6/969/2009/>
- Michalak, A. M., Hirsch, A., Bruhwiler, L., Gurney, K. R., Peters, W. and co-authors. 2005. Maximum likelihood estimation of covariance parameters for Bayesian atmospheric trace gas surface flux inversions. *J. Geophys. Res.* **110**, D24107. DOI: 10.1029/2005JD005970. Online at: <http://www.agu.org/pubs/crossref/2005/2005JD005970.shtml>
- Miles, N. L., Richardson, S. J., Davis, K. J., Lauvaux, T., Andrews, A. E. and co-authors. 2012. Large amplitude spatial and temporal gradients in atmospheric boundary layer CO₂ mole fractions detected with a tower-based network in the U.S. upper midwest. *J. Geophys. Res.* **117**(B), G01019. DOI: 10.1029/2011JG001781. Online at: <http://www.agu.org/pubs/crossref/2012/2011JG001781.shtml>
- Ogle, S., Breidt, F., Easter, M., William, S., Killian, K. and Paustian, K. 2010. Scale and uncertainty in modeled soil organic carbon stock changes for us croplands using a process-based model. *Glob. Change Biol.* **16**, 810–822. DOI: 10.1111/j.1365-2486.2009.01951.x. Online at: <http://onlinelibrary.wiley.com/doi/10.1111/j.1365-2486.2009.01951.x/abstract>
- Peters, W., Jacobson, A. R., Sweeney, C., Andrews, A. E., Conway, T. J. and co-authors. 2007. An atmospheric perspective

- on North American carbon dioxide exchange: CarbonTracker. *Proc. Natl Acad. Sci.* **104**(48), 18925–18930. DOI: 10.1073/pnas.0708986104. Online at: <http://www.pnas.org/content/104/48/18925.abstract>
- Raupach, M. R., LeQuéré, C. and Heimann, M. 2008. Anthropogenic and biophysical contributions to increasing atmospheric CO₂ growth rate and airborne fraction. *Biogeosciences* **5**, 1601–1613. DOI: 10.5194/bg-5-1601-2008. Online at: <http://www.biogeosciences.net/5/1601/2008/bg-5-1601-2008.html>
- Ricciuto, D., King, A., Dragoni, D. and Post, W. 2011. Parameter and prediction uncertainty in an optimized terrestrial carbon cycle model: effects of constraining variables and data record length. *J. Geophys. Res.* **116**, G01033. Online at: <http://www.agu.org/pubs/crossref/2011/2010JG001400.shtml>
- Rödenbeck, C., Houweling, S., Gloor, M. and Heimann, M. 2003. Time-dependent atmospheric CO₂ inversions based on inter-annually varying tracer transport. *Tellus B* **55**(2), 488–497.
- Rodgers, C. D. 2000. *Inverse Methods for Atmospheric Sounding: Theory and Practice*. World Scientific, Singapore.
- Schuh, A. E., Denning, A. S., Corbin, K. D., Baker, I. T., Uliasz, M. and co-authors. 2010. A regional high-resolution carbon flux inversion of North America for 2004. *Biogeosciences* **7**(5), 1625–1644. DOI: 10.5194/bg-7-1625-2010. Online at: <http://www.biogeosciences.net/7/1625/2010/>
- Schwalm, C. R., Williams, W. A., Schaefer, K., Anderson, R., Arain, M. A. and co-authors. 2010. A model-data intercomparison of CO₂ exchange across North America: results from the North American carbon program site synthesis. *J. Geophys. Res.* **115**, G00H05. DOI: 10.1029/2009JG001229. Online at: <http://www.agu.org/pubs/crossref/2010/2009JG001229.shtml>
- Uliasz, M. 1994. Lagrangian particle modeling in mesoscale applications. In: *Environmental Modelling II* (ed. P. Zanetti). Computational Mechanics Publications, Southampton, pp. 71–102.
- Wang, Y. P., Leuning, R., Cleugh, H. and Coppin, P. A. 2001. Parameter estimation in surface exchange models using nonlinear inversion: how many parameters can we estimate and which measurements are most useful? *Glob. Change Biol.* **7**, 495–510. Online at: <http://onlinelibrary.wiley.com/doi/10.1046/j.1365-2486.2001.00434.x/abstract>
- West, T. O., Bandaru, V., Brandt, C. C., Schuh, A. E. and Ogle, S. M. 2011. Regional uptake and release of crop carbon in the United States. *Biogeosciences* **8**, 631–654. Online at: <http://www.biogeosciences.net/8/2037/2011/bg-8-2037-2011.html>
- Wu, L., Bocquet, M., Lauvaux, T., Chevallier, F., Rayner, P. and Davis, K. 2011. Optimal representation of source-sink fluxes for mesoscale carbon dioxide inversion with synthetic data. *J. Geophys. Res.* **116**, D21304. Online at: <http://www.agu.org/pubs/crossref/2011/2011JD016198.shtml>